Positive Feedback Within a Kinase Signaling Complex Functions as a Switch Mechanism for NF-κB Activation

Hisaaki Shinohara *et al.*

Science **344**, 760 (2014);
DOI: 10.1126/science.1250020

zones dominated by SUP05 (*7*), revealed the presence of *rdsrA* and *rdsrC* genes (table S5), consistent with the prevalence of phage-encoded sulfur oxidation beyond hydrothermal plumes and in the wider pelagic oceans.

To date, deep-sea SUP05 has evaded growth in laboratory cultures; thus, direct host-phage manipulations and validation of the underlying mechanisms of phage-influenced sulfur oxidation remain a challenge. Yet, this study demonstrates the sequence-based elucidation of microbial community dynamics through the discovery of phages that infect a widespread deep-sea bacterium. The existence of *rdsr* genes in viral genomes reveals a mechanism for horizontal transfer of genes associated with sulfur cycling (*29*) and implicates viruses in the evolutionary dynamics of a central step in the planetary cycling of sulfur.

References and Notes

1. B. K. Swan *et al.*, *Science* **333**, 1296–1300 (2011).
2. J. Arístegui, J. M. Gasol, C. M. Duarte, G. J. Herndl, *Limnol. Oceanogr.* **54**, 1501–1529 (2009).
3. T. Reinthaler, H. M. van Aken, G. J. Herndl, *Deep-Sea Res. II* **57**, 1572–1580 (2010).
4. K. Anantharaman, J. A. Breier, C. S. Sheik, G. J. Dick, *Proc. Natl. Acad. Sci. U.S.A.* **110**, 330–335 (2013).
5. I. L. Newton *et al.*, *Science* **315**, 998–1000 (2007).
6. J. M. Petersen *et al.*, *Nature* **476**, 176–180 (2011).
7. D. A. Walsh *et al.*, *Science* **326**, 578–582 (2009).
8. D. E. Canfield *et al.*, *Science* **330**, 1375–1378 (2010).
9. S. Hara, I. Koike, K. Terauchi, H. Kamiya, E. Tanoue, *Mar. Ecol. Prog. Ser.* **145**, 269–277 (1996).
10. G. J. Dick, B. M. Tebo, *Environ. Microbiol.* **12**, 1334–1347 (2010).
11. R. A. Lesniewski, S. Jain, K. Anantharaman, P. D. Schloss, G. J. Dick, *ISME J.* **6**, 2257–2268 (2012).
12. G. J. Dick *et al.*, *Genome Biol.* **10**, R85 (2009).
13. S. R. Casjens *et al.*, *J. Bacteriol.* **187**, 1091–1104 (2005).
14. C. S. Sheik, S. Jain, G. J. Dick, *Environ. Microbiol.* **16**, 304–317 (2014).
15. M. Breitbart, L. R. Thompson, C. A. Suttle, M. B. Sullivan, *Oceanography* **20**, 135–139 (2007).
16. M. Breitbart, *Annu. Rev. Mar. Sci.* **4**, 425–448 (2012).
17. J. C. Ignacio-Espinoza, M. B. Sullivan, *Environ. Microbiol.* **14**, 2113–2126 (2012).
18. D. Lindell *et al.*, *Proc. Natl. Acad. Sci. U.S.A.* **101**, 11013–11018 (2004).
19. W. Ghosh, B. Dam, *FEMS Microbiol. Rev.* **33**, 999–1043 (2009).
20. D. Hensen, D. Sperling, H. G. Trüper, D. C. Brune, C. Dahl, *Mol. Microbiol.* **62**, 794–810 (2006).
21. K. T. Marshall, R. M. Morris, *ISME J.* **7**, 452–455 (2013).
22. D. Lindell, J. D. Jaffe, Z. I. Johnson, G. M. Church, S. W. Chisholm, *Nature* **438**, 86–89 (2005).
23. Materials and methods are available as supplementary materials on *Science* Online.
24. T. M. McCollom, *Deep-Sea Res. I* **47**, 85–101 (2000).
25. J. A. Breier *et al.*, *Geochim. Cosmochim. Acta* **88**, 216–236 (2012).
26. M. Li *et al.*, *Nat. Commun.* **5**, 3192 (2014).
27. S. Avrani, O. Wurtzel, I. Sharon, R. Sorek, D. Lindell, *Nature* **474**, 604–608 (2011).
28. B. L. Hurwitz, M. B. Sullivan, *PLOS ONE* **8**, e57355 (2013).
29. M. Klein *et al.*, *J. Bacteriol.* **183**, 6028–6035 (2001).

Acknowledgments: This project is funded in part by the Gordon and Betty Moore Foundation (grant GBMF2609) and the NSF (grants OCE1038006, OCE1038055, OCE1037991, and OCE1029242). We thank the University of Michigan Rackham Graduate School Faculty Research Fellowship Program for their support and M. Li and S. Jain for their assistance. DNA sequencing was conducted at the University of Michigan DNA Sequencing Core. We acknowledge the captain and crew of R/V *Thomas G. Thompson*, Chief Scientist A.-L. Reysenbach, and J. Sylvan for sampling and logistical support. For assistance with synchrotron measurements at BL10.3.2, we thank K. J. Edwards, J. V. Sorensen, M. A. Marcus, and S. C. Fakra. The Advanced Light Source is supported by the Director, Office of Science, Office of Basic Energy Sciences, of the U.S. Department of Energy (DOE) under contract no. DE-AC02-05CH11231. The nucleotide sequences are available from DOE JGI-IMG/MER (Taxon Object IDs: Kilo Moana, 3300001680; ABE, 3300001681; Mariner, 3300001678; Tahi Moana, 3300001679; Tui Malila, 3300001676; Guaymas, 3300001683) and the National Center for Biotechnology Information (BioProject: PRJNA234377). We declare no competing financial interests.

Supplementary Materials

www.sciencemag.org/content/344/6185/757/suppl/DC1
Materials and Methods
Supplementary Text
Figs. S1 to S10
Tables S1 to S6
References (*30*–*78*)
Data S1

14 February 2014; accepted 16 April 2014
Published online 1 May 2014;
10.1126/science.1252229

Positive Feedback Within a Kinase Signaling Complex Functions as a Switch Mechanism for NF-κB Activation

Hisaaki Shinohara,[1]* Marcelo Behar,[2,3]* Kentaro Inoue,[1] Michio Hiroshima,[4,5] Tomoharu Yasuda,[6]† Takeshi Nagashima,[1]‡ Shuhei Kimura,[7] Hideki Sanjo,[6]§ Shiori Maeda,[6] Noriko Yumoto,[1] Sewon Ki,[1] Shizuo Akira,[8] Yasushi Sako,[5] Alexander Hoffmann,[2,3]‖ Tomohiro Kurosaki,[6,9]‖ Mariko Okada-Hatakeyama[1]‖

A switchlike response in nuclear factor–κB (NF-κB) activity implies the existence of a threshold in the NF-κB signaling module. We show that the CARD-containing MAGUK protein 1 (CARMA1, also called CARD11)–TAK1 (MAP3K7)–inhibitor of NF-κB (IκB) kinase-β (IKKβ) module is a switch mechanism for NF-κB activation in B cell receptor (BCR) signaling. Experimental and mathematical modeling analyses showed that IKK activity is regulated by positive feedback from IKKβ to TAK1, generating a steep dose response to BCR stimulation. Mutation of the scaffolding protein CARMA1 at serine-578, an IKKβ target, abrogated not only late TAK1 activity, but also the switchlike activation of NF-κB in single cells, suggesting that phosphorylation of this residue accounts for the feedback.

The transcription factor nuclear factor-κB (NF-κB) has a central role in determining cellular outcomes (*1*–*3*). Stimulus-driven NF-κB activity is highly dynamic and shows oscillations due to transcriptionally inducible negative feedback of inhibitor of NF-κB (IκB) (*3*–*6*). When examined at the single-cell level, NF-κB activity is triggered in a switchlike manner, and the number of fully activated cells underlies a shallow population dose response (*6*). The switchlike response in NF-κB activity implies the existence of a threshold in the receptor-proximal signaling module, but this mechanism has not been elucidated.

In B cell receptor (BCR) signaling, NF-κB activity determines multiple B cell functions (*7*) (Fig. 1A). BCR stimulation by cognate antigen first induces activation of protein kinase C β (PKCβ), which phosphorylates serine-668 (S668) of CARD-containing MAGUK protein1 (CARMA1, also called CARD11). This modification causes a conformational change in CARMA1, allowing recruitment and activation of both the protein

[1]Laboratory for Integrated Cellular Systems, RIKEN Center for Integrative Medical Sciences (IMS-RCAI), Tsurumi-ku, Yokohama, Kanagawa 230-0045, Japan. [2]Signaling Systems Laboratory, Department of Chemistry and Biochemistry, University of California, San Diego, La Jolla, CA 92093, USA. [3]Institute for Quantitative and Computational Biosciences (QC Bio) and Department of Microbiology, Immunology, and Molecular Genetics, University of California, Los Angeles, Los Angeles, CA 90025, USA. [4]Laboratory for Cell Signaling Dynamics, RIKEN Quantitative Biology Center (QBiC), 6-2-3, Furuedai, Suita, Osaka 565-0874, Japan. [5]Cellular Informatics Laboratory, RIKEN, 2-1 Hirosawa, Wako 351-0198, Japan. [6]Laboratory for Lymphocyte Differentiation, RIKEN Center for Integrative Medical Sciences (IMS-RCAI), Tsurumi-ku, Yokohama, Kanagawa 230-0045, Japan. [7]Graduate School of Engineering, Tottori University 4-101, Koyama-minami, Tottori 680-8552, Japan. [8]Laboratory of Host Defense, WPI Immunology Frontier Research Center, Osaka University, 3-1 Yamada-oka, Suita, Osaka 565-0871, Japan. [9]Laboratory for Lymphocyte Differentiation, WPI Immunology Frontier Research Center, Osaka University, 3-1 Yamada-oka, Suita, Osaka 565-0871, Japan.

*These authors contributed equally to this work.
†Present address: Max-Delbrück-Center for Molecular Medicine, 13125 Berlin, Germany.
‡Present address: Division of Cell Proliferation, Tohoku University Graduate School of Medicine, Sendai, Miyagi 980-8575, Japan.
§Present address: Department of Molecular and Cellular Immunology, Shinshu University School of Medicine, 3-1-1 Asahi, Matsumoto, Nagano 390-8621 Japan.
‖Corresponding author. E-mail: ahoffmann@ucla.edu (A.H.); kurosaki@rcai.riken.jp (T.K.); marikoh@rcai.riken.jp (M.O-H)

kinase TAK1 (also called MAP3K7) and the adapter protein Bcl10, the caspase-like protein MALT1 (CBM complex), and the associated IκB kinase (IKK) complex (*7*, *8*). These interactions cause IKKβ activation, allowing for IκB phosphorylation and degradation, resulting in nuclear translocation of NF-κB and increased transcription of target genes. The assembly of the CARMA1 complex is regulated via multiple mechanisms (*9*–*12*). Notably, the activated IKKβ phosphorylates CARMA1 at S578, thereby serving as a positive modifier to enhance the assembly of the CARMA1 complex, which increases IKKβ activity (*13*). Regulatory motifs involving positive feedback may enhance and prolong stimulus-induced activities and, in some cases, provide the basis for switchlike behavior in signaling pathways (*14*, *15*). We used iterative quantitative experiments and mathematical modeling to show that TAK1-IKKβ engages in positive feedback through CARMA1 and that this positive feedback loop can produce switchlike activation of NF-κB.

TAK1 may be critical for induction of NF-κB activity through the regulation of IKK activity (*7*). Indeed, we found that upon BCR stimulation, splenic B cells obtained from mice after conditional deletion of TAK1 (TAK1-cKO) showed very little nuclear translocation of RelA and NF-κB1 (fig. S1A), IKKβ activation, phosphorylation of IκB (fig. S1, B and C), and expression of NF-κB target genes (e.g., *Fas*, *A20*, and *Il10*) (Fig. 1, B and C). Steep induction of cellular proliferation in response to stronger stimuli observed in wild-type cells [Hill coefficient,1.88; median effective concentration (EC_{50}), 1.46×10^{-6} g/ml] was abolished in the TAK1-cKO cells (Fig. 1D). Thus, TAK1 appears to be indispensable for BCR-mediated activation of NF-κB and cell proliferation.

To further investigate the regulation of NF-κB activity in response to BCR-stimulation, we assessed TAK1 and IKKβ activities in chicken DT40 B cells. We used an ultrafine, 90-s-interval time-course analysis of TAK1 activity to resolve two maxima at 1.5 and 6 min after BCR stimulation (Fig. 2A and fig. S2A). By contrast, IKKβ activity showed an initial plateau followed by a peak at 6 min (Fig. 2B and fig. S2B). When knock-in

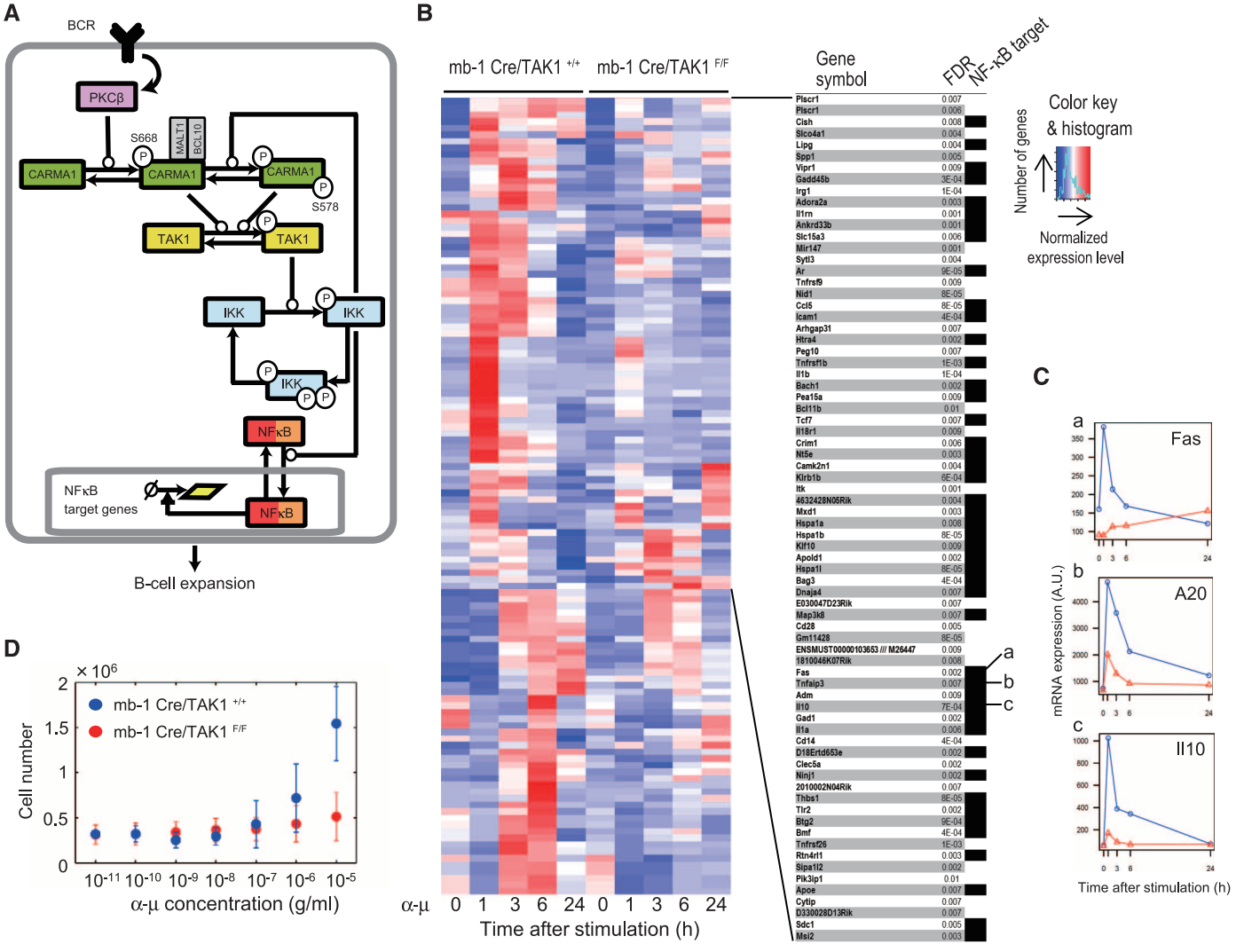

Fig. 1. IKKβ-NF-κB activation in BCR signaling. (**A**) The NF-κB activation pathway in BCR signaling. The circled letter P indicates phosphorylated state of the amino acid residue. Arrows show functional modifications of the protein or protein complex. Lines ended by an open circle indicate activation of the component. (**B** to **D**) Role of TAK1 in NF-κB activation in mouse primary B cells. (B) Gene expression analysis. Splenic B cells from control mice (mb-1Cre/TAK1$^{+/+}$) or TAK1 B cell knockout mice (mb-1Cre/TAK1$^{F/F}$) were stimulated with anti-IgM (10 μg/ml) (α-μ) for the indicated time periods. Up-regulated genes in control mice with compatible genes in TAK1 knockout mice are shown. NF-κB target gene is shown as a black box (NF-κB target), and *Fas* (a), *A20* (b), and *Il-10* (c) represent typical target genes. FDR, false discovery rate. (**C**) TAK1-deficient splenic B cells showed significantly decreased expression of typical NF-κB-target genes; *Fas* (a), *A20* (b), and *Il-10* (c) in response to anti-IgM (α-μ) stimulation; control (blue), TAK1 knockout (red). (**D**) B cell proliferation dose response. Data are mean ± SD [n = 5 mice for control (blue); n = 3 mice for TAK1 knockout (red)].

cells expressing catalytically inactive IKKβ ($IKK\beta^{SSAA}$, S176A and S181A mutated) B cells (*13*) were examined, TAK1 activity was significantly reduced and the second peak was completely absent (Fig. 2A and fig. S2A). Mutation of IKKβ also decreased the interaction of TAK1 with CARMA1 (fig. S3, A and C). The lack of correspondence between time-course patterns of TAK1 and IKKβ activities, as well as the reduced TAK1 activity in $IKK\beta^{SSAA}$ cells, hinted at a positive-feedback regulation from IKKβ to TAK1.

To rigorously analyze the observed signaling dynamics, we constructed a mathematical model depicting the activity states of TAK1 and IKKβ with phosphorylation of CARMA1 S668 (P668) as an input (Fig. 2C and fig. S4). The model includes two IKKβ activation states, IKK2 and IKK3 (potentially reflecting oligomerization or different phosphorylation states), whose formation is mediated by trans-autophosphorylation (*16*), and an inactivated form (IKK4) likely mediated by further phosphorylation and subsequent breakdown of the complex containing NF-κB essential modifier (IKKγ, also called NEMO) (*17*) (Fig. 2C and table S1). In the absence of IKKβ self-activation and phosphorylation processes, the model failed to show late TAK1 and IKKβ activities and termination of the signals, respectively (fig. S5). After parameterization, the model simulations showed an excellent correspondence with the experimental time course (Fig. 2, D and E, and fig. S2) and dose-response profiles (Fig. 2, F and G, and figs. S6 and S7) of TAK1 and IKKβ activity. The high Hill coefficient of IKKβ at 6 min but not at 1.5 min (1.92 and 0.34, respectively; EC_{50}, 1.83×10^{-7} g/ml) in dose-response profiles is characteristic of a positive-feedback regulation.

Analysis of the model trajectory in the phase space showed that TAK1 operates close to quasi-equilibrium and that its initial activity is mainly driven by the input signal (but still helped by IKK

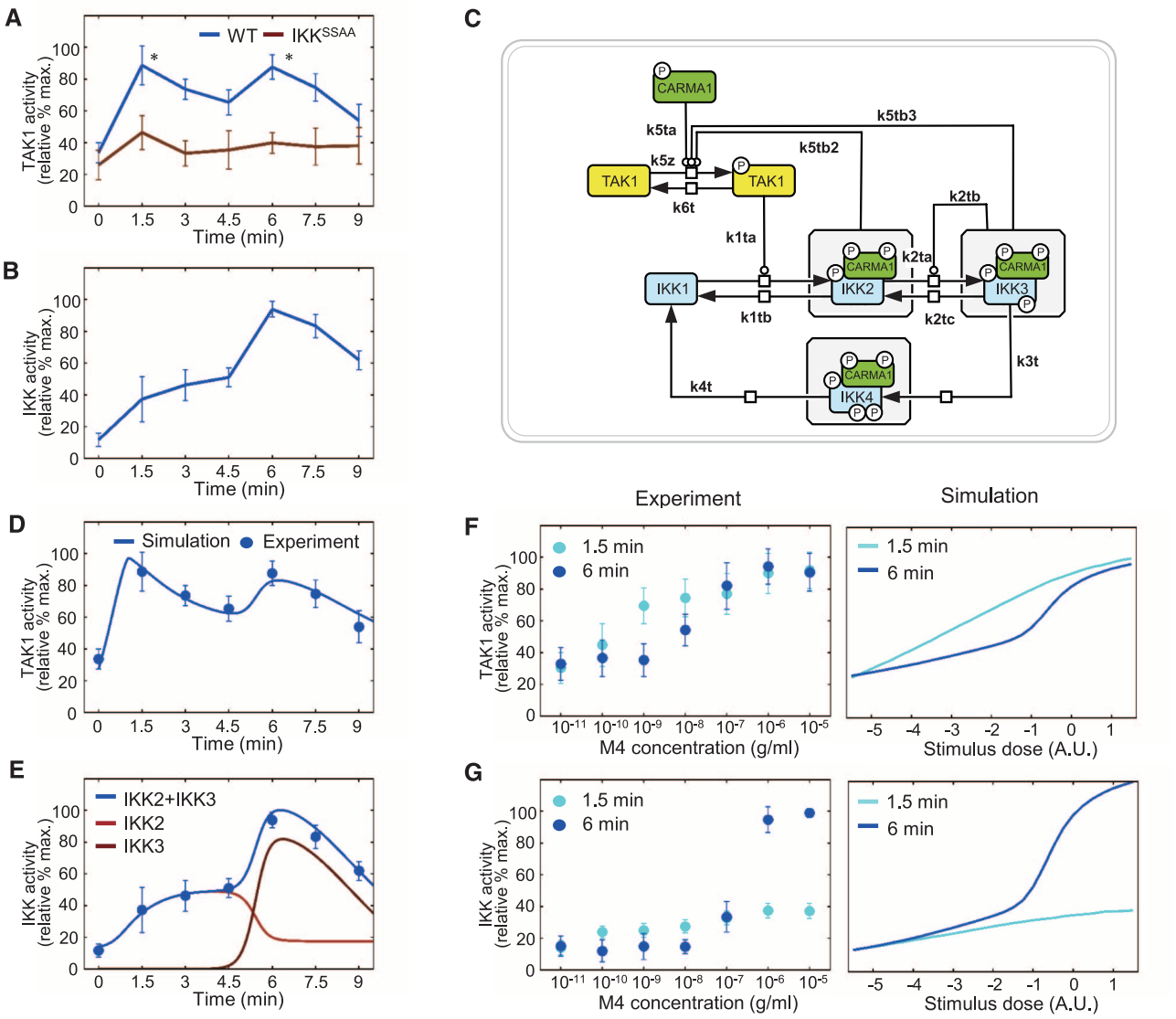

Fig. 2. Mathematical model of TAK1-IKKβ positive feedback. (**A**) Time course of TAK1 activity in DT40 B cells after stimulation with the monoclonal antibody (mAb) to chicken IgM (M4). Results are mean ± SD ($n = 8$). Wild type (WT, blue), IKK^{SSAA} (brown). * denotes statistical significant difference ($P < 0.01$, Welch's *t* test) from the value at 4.5 min. (**B**) Time course of IKKβ activity after stimulation with M4. Results are mean ± SD ($n = 6$). (**C**) Diagram of the TAK1-IKKβ feedback model. Each activation state of IKKβ is depicted: IKK1 (basal), IKK2 (phosphorylated), IKK3 (trans-activated, highly active), and IKK4 (hyper-phosphorylated, inactive). Parameters shown on the arrows correspond to those in the sensitivity analysis in Fig. 3, B and C. The circled letter P denotes phosphorylation state. Lines with an open circle represent activation. (**D** and **E**) Simulation (lines) and experimental data (dots) of the time-course responses. Values of TAK1 (D) and IKKβ (E) activities are shown as median relative to the maximum change measured in M4-stimulated cells, so that the maximum values equal 100 (see fig. S2 and supplementary methods) ($n = 8$). (**F** and **G**) Experimental (dots) and simulation (lines) data of dose responses. TAK1 (F) and IKKβ (G) activities were examined at 1.5 (aqua) and 6 min (blue) after stimulation with the indicated concentrations of M4 ($n = 8$ to 10).

activity) but becomes driven by IKKβ as the event progresses (Fig. 3A). This explains loss of the second peak of TAK1 activity and reduced initial peak in IKKβ^{SSAA} cells (Fig. 2A). The model predicted that late TAK1 activity is only possible in the presence of persistent input signal (Fig. 3A, right), which is consistent with the loss of the second peak in the presence of a PKC inhibitor after 2 min of BCR stimulation (fig. S8). Likewise, IKK2 activation mediated by the TAK1 activity (k1ta) is the most sensitive parameter for IKKβ activation (Fig. 3B). A positive-feedback loop from IKK3 to TAK1 (k5tb3) controls the amplitude of IKKβ and late TAK1 activities (Fig. 3C). We confirmed in mouse splenic B cells that the second wave of TAK1 activity was abolished by addition of an IKKβ inhibitor (BAY11-7985) after 2 min of BCR stimulation (Fig. 3D, fig. S9, and table S2). These results suggest that the IKKβ-mediated sustained activation of TAK1 is a common mechanism for TAK1 activation. Thus, IKKβ activity is essential for the steep dose response of TAK1 activity (Fig. 3E and fig. S6).

Deletion of TAK1 severely reduced phosphorylation of S578 in CARMA1 (fig. S3, B and F), without having any effect on the PKCβ-dependent phosphorylation of S668 (fig. S10), suggesting that an upstream feedback target is unlikely. By contrast, the second peak of TAK1 activity was completely abrogated in this CARMA1^{S578A} mutant (Fig. 3F and fig. S11). Suppressing the IKKβ-driven feedback in the mathematical model resulted in a TAK1 activity profile that recapitulated the experimental data (Fig. 3F and table S3).

We investigated the role of the Bcl10 adaptor protein in the CARMA1 complex for IKK-dependent TAK1 activation. Bcl10 positively regulates NF-κB activation in antigen receptor signaling (*18*); however, negative regulation of Bcl10 by IKKβ is also implicated after T cell receptor (TCR) engagement (*10*–*12*). The time course profile of TAK1 activity in Bcl10$^{-/-}$ cells (fig. S12) was similar to that of IKKβ^{SSAA} cells (Figs. 2A and 3G and fig. S2), suggesting that Bcl10 has a positive role in IKKβ feedback regulation in this time frame. However, the overall reduction of TAK1 activity in these mutants raised the additional possibility that both Bcl10 and IKKβ may facilitate the initial activation of TAK1. Simulations with attenuated inputs of both CARMA1-P668 and IKKβ feedback (table S4) recapitulated

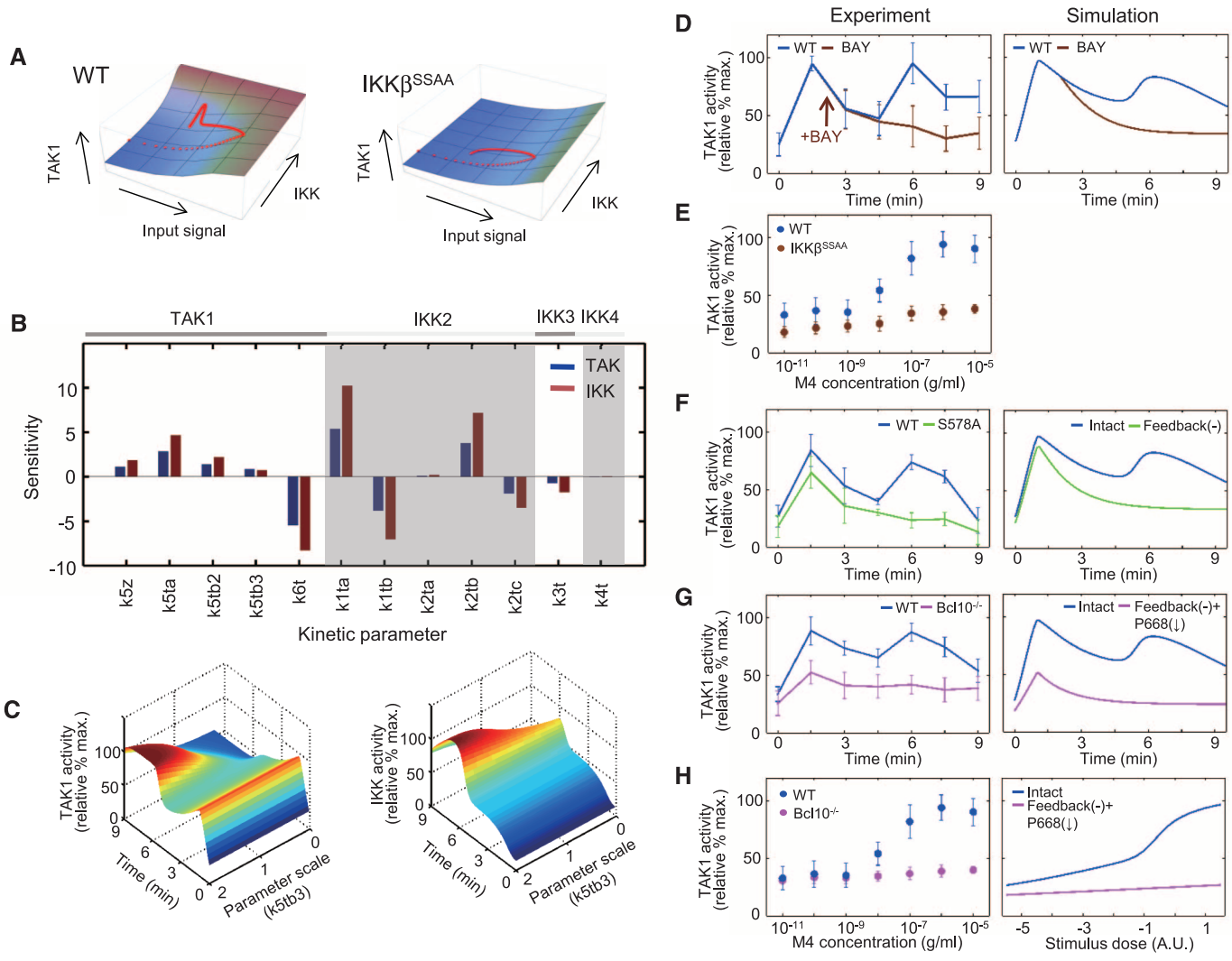

Fig. 3. Role of TAK1-IKKβ feedback loop in switchlike activation of TAK1 and IKKβ. (**A**) Equilibrium surface of TAK1 activity in WT and IKKβ^{SSAA} cells obtained by simulation. (**B**) Sensitivity analysis of TAK1 activity and IKKβ activity on each kinetic parameter. (**C**) Simulated effects of various degrees (0.02 to 2 times that of the wild type) of the positive-feedback strength (k5tb3) from IKK3 to TAK1 on TAK1 (left) and IKKβ (right) activities. (**D**) Time course of TAK1 activity in mouse B cells. The IKKβ inhibitor BAY11-7085 (BAY) was added 2 min after stimulation with anti-IgM (10 μg/ml) (left). The simulation represents the attentuation of IKKβ 2 min after signal input (right). (**E**) TAK1 dose response from experimental data in WT and IKKβ^{SSAA} cells at 6 min after ligand stimulation (n = 8 to 10). (**F**) Time-course experiment of TAK1 activation in WT and CARMA1^{S578A} DT40 B cells (n = 3) (left). Simulation of TAK1 time-course activities under feedback attenuated conditions (right). (**G**) Time-course experiment of TAK1 activation in WT and Bcl10$^{-/-}$ DT40 B cells (n = 8) (left). Simulation of TAK1 time-course activities under feedback and input attenuated conditions (right). (**H**) Experimental data for TAK1 activity in an M4 dose-response study in Bcl10$^{-/-}$ cells (n = 8) (left). Simulation of the dose response of TAK1 activities under feedback and input attenuated conditions (right).

the time-course dynamics of TAK1 activity in Bcl10$^{-/-}$ cells (Fig. 3G and fig. S2A). The model's dose response of TAK1 activity to BCR stimulation in this hypothetical condition accurately captured the experimental observations in the Bcl10$^{-/-}$ (Fig. 3H and fig. S13) and IKKβ^{SSAA} cells (Fig. 3E and fig. S6). In support of the simulation, phosphorylation of CARMA1 at S668 (input signal) was reduced in cells deficient in IKKβ or Bcl10 (fig. S14). Bcl10 and MALT1 binding in the CARMA1 complex was also reduced in the IKKβ-deficient cells (fig. S3, B to E). Taken together, these data indicate that Bcl10 and IKKβ mediate feedback regulation of TAK1, but may also function in initial activation of TAK1 in the CARMA1 complex, as shown in T cells (*10*).

To determine whether the CARMA1-TAK1-IKKβ positive-feedback loop that functions to amplify IKKβ activity in BCR signaling also functions to induce switchlike activation of NF-κB, we examined nuclear translocation of RelA in cell populations (fig. S15A). In the steep dose-dependent RelA translocation profile at 45 min, peak maxima exhibited positive cooperativity (Hill coefficient, 2.46; EC_{50}, 1.48×10^{-6} g/ml) (Fig. 4B and fig. S15C) and closely resembled that of the IKKβ activity at 6 min (Fig. 4A). The analysis showed that the dose response of RelA translocation is shifted and more gradual in the CARMA1 S578 mutant cells (Fig. 4B and fig. S15C), suggesting a lack of positive cooperativity in this mutant.

We tested whether the switchlike activation of NF-κB observed at the cell population level also existed at the single-cell level. Live cell images showed that the RelA labeled with green fluorescent protein (GFP) in the cytosol in the resting state began to translocate into the nucleus at 10 min after BCR stimulation and remained until ~60 min in wild-type cells (Fig. 4C). Activated cells showing a high ratio of nuclear to cytosolic (N/C > 1) RelA-GFP were observed under various dosage conditions, although the frequency of such active cells decreased along with decreased concentrations of antibodies against immunoglobulin M (anti-IgM) (10^{-4} g/ml, 78%; 10^{-5} g/ml, 90%; 10^{-6} g/ml, 64%; 10^{-7} g/ml, 26%; 10^{-8} g/ml, 20%) at 45 min after BCR stimulation (Fig. 4D). The apparent Hill coefficient was 7.03 (EC_{50}, 9.1×10^{-7} g/ml) for wild type, whereas CARMA1^{S578A} mutant cells exhibited a more graded response even at high antibody concentrations.

Our study provides evidence that the TAK1-IKKβ positive-feedback loop mediated by phosphorylation of CARMA1 at S578 serves as a basis for switchlike activation of NF-κB, thereby determining an activation threshold in BCR signaling. A switchlike response is not always produced by simple positive feedback. Additional conditions, such as low activity before stimulation, should also be met to produce a large difference in the kinetic rates (*19*). The stoichiometry of the CARMA1 scaffolding protein and the binding kinases must also be optimal to present a switchlike effect (*20*, *21*). By this means, various modifications of CARMA1 may allow different thresholds of NF-κB to be set and thereby shape NF-κB signaling dynamics.

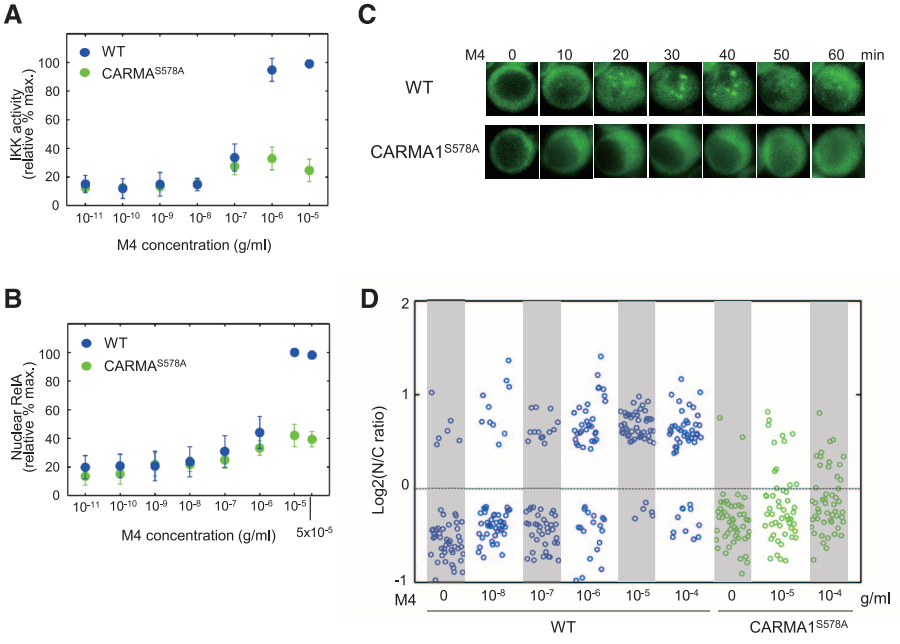

Fig. 4. Switchlike activation of NF-κB at population and single-cell levels. (**A**) Dose response of IKKβ activation. IKKβ activities were measured in WT (blue) and CARMA1^{S578A} (green) DT40 B cells ($n = 5$) by kinase assay at 6 min after stimulation with the indicated concentration of mAb to chicken IgM (M4). (**B**) Dose response of NF-κB activation. NF-κB activity was examined in WT (blue) and CARMA1^{S578A} (green) DT40 B cells ($n = 5$) by RelA translocation into the nucleus at 45 min after stimulation with the indicated concentration of M4. (**C** and **D**) Single-cell imaging analysis of GFP-tagged RelA nuclear translocation. (C) A representative time-course response in WT (top) and CARMA1^{S578A} (bottom) cells. Live-cell snapshots up to 60 min after M4 (10^{-5} g/ml) stimulation. (D) Dose response. Cells were stimulated with M4 at the indicated concentration in WT (blue) and CARMA1^{S578A} (green) cells. Nuclear-to-cytoplasmic ratio (N/C) of fluorescence at 45 min after stimulation was calculated (50 cells per experiment).

References and Notes

1. M. S. Hayden, S. Ghosh, *Genes Dev.* **26**, 203–234 (2012).
2. S. Basak, M. Behar, A. Hoffmann, *Immunol. Rev.* **246**, 221–238 (2012).
3. L. Ashall *et al.*, *Science* **324**, 242–246 (2009).
4. A. Hoffmann, A. Levchenko, M. L. Scott, D. Baltimore, *Science* **298**, 1241–1245 (2002).
5. T. Y. Tsai *et al.*, *Science* **321**, 126–129 (2008).
6. S. Tay *et al.*, *Nature* **466**, 267–271 (2010).
7. H. Shinohara, T. Kurosaki, *Immunol. Rev.* **232**, 300–318 (2009).
8. M. Thome, J. E. Charton, C. Pelzer, S. Hailfinger, *Cold Spring Harb. Perspect. Biol.* **2**, a003004 (2010).
9. R. L. Lamason, A. Kupfer, J. L. Pomerantz, *Mol. Cell* **40**, 798–809 (2010).
10. E. Wegener *et al.*, *Mol. Cell* **23**, 13–23 (2006).
11. C. Lobry, T. Lopez, A. Israël, R. Weil, *Proc. Natl. Acad. Sci. U.S.A.* **104**, 908–913 (2007).
12. H. Zeng *et al.*, *Mol. Cell. Biol.* **27**, 5235–5245 (2007).
13. H. Shinohara, S. Maeda, H. Watarai, T. Kurosaki, *J. Exp. Med.* **204**, 3285–3293 (2007).
14. S. D. Santos, P. J. Verveer, P. I. Bastiaens, *Nat. Cell Biol.* **9**, 324–330 (2007).
15. J. E. Ferrell Jr., E. M. Machleder, *Science* **280**, 895–898 (1998).
16. S. Polley *et al.*, *PLOS Biol.* **11**, e1001581 (2013).
17. H. Häcker, M. Karin, *Sci. STKE* **2006**, re13 (2006).
18. J. Ruland *et al.*, *Cell* **104**, 33–42 (2001).
19. A. J. Ninfa, A. E. Mayo, *Sci. STKE* **2004**, pe20 (2004).
20. A. Levchenko, J. Bruck, P. W. Sternberg, *Proc. Natl. Acad. Sci. U.S.A.* **97**, 5818–5823 (2000).
21. E. C. O'Shaughnessy, S. Palani, J. J. Collins, C. A. Sarkar, *Cell* **144**, 119–131 (2011).

Acknowledgments: We thank T. Takemori, M. Nomura, S. Magi, A. Imamoto, and P.D. Burrows for advice and review of the manuscript and M. Reth for providing mb1-Cre mice. The study is supported by a RIKEN RCAI project for Interdisciplinary Research to H.S., and in part by Cell Innovation Program, Ministry of Education, Culture, Sports, Science and Technology, Japan and the Aihara Innovative Mathematical Modelling Project, FIRST program, Japan Society for the Promotion of Science, to M.O.-H. M.B. was funded by a Postdoctoral Research Fellowship from the Cancer Research Institute and NIH grant 5R01CA141722 to A.H. The microarray data are deposited at Gene Expression Omnibus under accession number GSE41176. The authors declare no competing financial interests. H.S. designed the research; H.S., T.Y., S.M., N.Y., and S.K. performed the experiments; M.B., K.I., and S.K. performed computational analysis; H.S., M.H, and Y.S. performed single-cell imaging analysis; T.N. analyzed the microarray data; H.S. and S.A. provided essential reagents; H.S., M.B., K.I., and M.O.-H. analyzed the data; H.S., M.B., K.I., A.H., and M.O.-H. wrote the paper; and A.H., T.K., and M.O-H. conceived the study and provided overall direction.

Supplementary Materials

www.sciencemag.org/content/344/6185/760/suppl/DC1
Materials and Methods
Figs. S1 to S15
Tables S1 to S4
References (*22*–*34*)

20 December 2013; accepted 16 April 2014
10.1126/science.1250020